Anal Bioanal Chem (2010) 396:163–172
DOI 10.1007/s00216-009-2919-1

ORIGINAL PAPER

Material ejection and redeposition following atmospheric pressure near-field laser ablation on molecular solids

Liang Zhu · Gerardo Gamez · Thomas A. Schmitz · Frank Krumeich · Renato Zenobi

Received: 23 March 2009 / Revised: 13 June 2009 / Accepted: 15 June 2009 / Published online: 7 July 2009

Abstract Near-field laser ablation (NF-LA) coupled with mass spectrometry (MS) is very promising for highly spatially resolved chemical analyses on various substrates at atmospheric pressure, for example, in materials and life science applications. Although nanoscale sample craters can be produced routinely, no molecular mass spectra of ablated material from craters of ≤1 μm diameter have ever been acquired by NF-LA MS at atmospheric pressure. Some of the pressing questions are thus how much of the ablated material is transported into the mass spectrometer and in what form. Therefore, material redeposition on the near-field tip's surface from laser ablation of molecular solids was characterized with scanning electron microscopy. The crater profiles were studied by scanning probe microscopy. The results shown in this study demonstrate that there could be as much as 70% of the ablated material deposited on the near-field tip's surface. The redeposited products were found to be confined to a height of ~50 μm, thus suggesting that most components inside near-field ablation plumes propagate about the same distance for both anthracene and tris(8-hydroxyquinolinato)aluminum. Nanoparticles ablated from craters of ≤1 μm diameter are clearly observed. Furthermore, observation of tips after ablation of an anthracene surface angled at 60° with respect to a horizontal surface shows that the direction of the near-field ablation plume is neither in the direction of the surface normal nor towards the axis of incident laser beam but deflected further away from surface normal.

Keywords Near field · Laser ablation · Molecular solids · Atmospheric pressure · SEM

Liang Zhu and Gerardo Gomez contributed equally to this article.

L. Zhu · G. Gamez · T. A. Schmitz · R. Zenobi (✉)
Department of Chemistry and Applied Biosciences, ETH Zürich, 8093 Zürich, Switzerland
e-mail: zenobi@org.chem.ethz.ch

F. Krumeich
Laboratory of Inorganic Chemistry, ETH Zürich, 8093 Zürich, Switzerland

Introduction

Techniques capable of acquiring both the topographic and chemical information of samples at the nanoscale are of great importance for progress in materials and life science research. Recently, various spectroscopic techniques, including Raman spectroscopy [1–3] combined with scanning probe microscopy (SPM) [4] and fluorescence spectroscopy [5, 6], have been shown to be suitable for nanoscale chemical analysis. However, the ability to provide broad chemical information and the possibility to perform depth profiling render the combination of mass spectrometry (MS) with nanoscale laser ablation (LA) one of the most promising candidates [7]. Traditionally, far-field laser ablation MS techniques for molecular analysis at atmospheric pressure (AP) can provide a spatial resolution around 50–100 μm [8, 9] and 25–40 μm in the case of oversampling techniques [10]. Recently, a custom-built scanning microprobe AP matrix-assisted laser desorption/ionization ion source has achieved a spatial resolution around 3×1.2 μm using highly coaxial laser focusing, when it is coupled to a linear ion trap MS [11]. Better spatial resolution has so far only been achieved in high-vacuum systems with techniques such as specially designed detectors/ion optics or by secondary ion mass spectrometry [12–18]. The difficulty of manipulating samples, especially fragile biological samples, in the high-vacuum environment provides a key motivation for the development of laser ablation MS techniques working at ambient conditions.

The theoretical diffraction limit ($\lambda/2$) which hinders high-resolution laser ablation MS can be overcome by scanning near-field optical microscopy (SNOM) [4]: by coupling a pulsed UV laser into the far end of an aperture probe which acts as a nanolight source, craters as small as 70 nm can be produced on anthracene and rhodamine thin film [19, 20]. Also, the optical antenna effect ("apertureless SNOM") is capable of ablating material from an area of a diameter as small as 10 nm [21, 22]. It has been demonstrated that combining laser ablation with apertureless SNOM and inductively coupled plasma mass spectrometry (LA-ICP MS) at ambient pressure yields elemental analysis of metallic alloy standards on the hundred nanometer scale [23, 24]. However, during these "near-field" laser ablation experiments, the distance of the tip to the sample surface was so large (~200 nm) [24] that this is certainly no near-field effect. In 2008, based on a previous quadrupole-mass-spectrometer-based setup [25], a new instrument that combines near-field laser ablation through SNOM probes at ambient pressure with an ion trap/time of flight mass spectrometer [26] was successfully applied in our laboratory to analyze molecular signals from an anthracene surface, with a lateral resolution of ~5 μm [27]. The ultimate goal, however, is to acquire molecular mass spectra on the nanoscale together with the corresponding topographical information.

Indeed, craters well below the diffraction limit can be created reproducibly, but no molecular mass spectra of ablated material at nanoscale have ever been acquired at ambient pressure [11, 19, 21, 22]. Of course, smaller craters yield less ablated material available for analysis, thus demanding a very high sensitivity mass spectrometer [11]. For example, let us take a crater with 1 μm diameter and ~0.5 μm depth. The total ablated material from a cone-shaped volume with these dimensions is around 1.3×10^{-19} m^3, corresponding to 0.9 fmol for the case of anthracene. Besides this fact, there is little knowledge known about the nature and the spatial distribution of material ablated from near-field laser ablation events. This information could be instructive in general and important to improve the sensitivity of near-field laser ablation mass spectrometry (NF-LA MS), i.e., by increasing the collection efficiency.

A wide variety of far-field laser ablation studies have been performed on various substrates to observe the correlation between irradiation conditions, laser pulse width, laser profiles, ablated products, and the size and shape of the craters [28–33]. For example, it has been reported that ultrashort pulses (e.g., femtosecond lasers) cause less collateral damage than longer pulses [33]. Great attention has been paid to the form, composition, and size of ablation products from different substrates under typical laser ablation conditions for LA-ICP mass spectrometry [34–41]. In addition, the fundamental chemical and physical processes (ablation mechanisms) underlying the laser ablation phenomenon have been studied based on theoretical simulations [28, 42–44]. Various mechanisms of material ejection during laser ablation events including surface desorption, phase explosion, photomechanical effects, and photochemical effects have been proposed. The predominance of a certain ablation mechanism depends on the irradiation conditions [43]. Among them, one theory proposes that a "slow" plume component of larger clusters or particles remains close to the sample surface even at timescale of several tens of microseconds after laser pulse, whereas a "fast" component consisting of gaseous neutrals and tiny clusters is observed at larger distance [42, 45, 46]. For the case of far-field laser ablation, both experimental evidence and theoretical predictions show that (1) particles and clusters are produced in most (if not all) LA events, either from condensation (in the plume or directly from a molten area) or photomechanically depending on the laser parameters; (2) that the height of the ablation plume can be several hundreds of micrometers or even in the millimeter range; and (3) that the propagation of the plume on tilted substrate surfaces usually does not follow the direction of incident laser beam but is normal to the substrate surface. A key question for near-field laser ablation events at ambient pressure therefore is whether or not these findings will also apply, especially for the case of molecular solids. Furthermore, during a near-field laser ablation event, the SNOM tip, which normally has a footprint of around 200–300 nm in diameter, is held within 10 nm of the laser ablation site. A violent interaction of the ablation plume with the tip itself seems unavoidable. Thus, possible redeposition of ablated material on the tip surface (and if so, how much?) [19] and the influence of tip heating induced by the laser energy needs to be clarified.

In this study, aperture SNOM tips were characterized by SEM after a certain number of laser ablation events, and corresponding crater profiles were measured using SPM. Several differences between near-field and far-field laser ablation were observed through a systematic study of two molecular solids under various experimental parameters.

Experimental section

The SNOM probes for near-field laser ablation were produced following the "tube etching" method [47]. A multimode silica fiber with good UV transmission (attenuation 70 dB/km at 350 nm) was used as the raw material for the fabrication of all SNOM tips (multimode UV-vis, 50 μm core diameter, 125 μm cladding diameter, 250 μm acrylate jacket, from Fiberguide Industries, Stirling, NJ, USA). Following taper

formation by etching in 40% hydrofluoric (HF) with an overlayer of isooctane for 120 min at room temperature, the acrylate fiber jacket was normally removed by hot H_2SO_4 (120 °C), and the fiber was washed with ethanol and deionized water and then dried and stored [47]. As shown below, the SNOM tips etched at room temperature have a fairly narrow cone angle. In order to fabricate wider cone angle tips that exhibit higher optical throughput [48] and better mechanical stability, the fibers were etched with 40% aqueous HF at higher temperature (from 20 to 60 °C) for 60 min. Afterwards, tips were mounted on a tuning fork assembly that has a frequency of 32.768 kHz. A frequency-tripled, Q-switched Nd:YLF UV laser (349 nm, <15 ns nominal pulse width, Triton, Spectra Physics, Mountain View, CA, USA) was coupled into the blunt end of the SNOM fiber, whose tip end was kept in feedback close to the sample surface by a commercial SNOM instrument (Topometrix Lumina, Veeco Metrology Inc., Santa Barbara, CA, USA) equipped with a shear-force scan head (maximum piezo range 100×100 μm). For individual tips, the optimum value of laser energy required to generate submicrometer craters reproducibly needs to be determined. The desired surface area before and after laser ablation was scanned using SNOM tips in shear force feedback to acquire topographic information of craters. Laser ablation by either single shots or bursts of several shots were controlled by a pulse/delay generator (model 555, Berkeley Nucleonics Corporation, San Rafael) and homemade burst generator. Hundreds of laser ablations were performed on the surface of a sample pellet, either by continuous laser ablation at a given repetition rate during tip scanning (scan rate 10 μm/s, 100×100 pixels, pixel size 0.1 μm) or in a point-to-point mode. The "point-to-point mode" refers to performing laser ablation at individual sample locations by moving the SNOM tip from one spot to another. The morphology of the tips before and after hundreds of laser shots was characterized using SEM. The tips were investigated as received with a Gemini 1530 FEG microscope (Zeiss) at low voltage (0.8–1 keV) to minimize the charging effects. The laser pulse energy exiting the tip end was directly measured by a picojoule power meter (PD 10-pJ, Ophir Optronics Ltd., Jerusalem, Israel), while the tip was approached to the active surface of the picojoule meter. The measured laser pulse energies from three representative tips were correlated to the laser pulse energies coupled into the blunt end of the fiber tips. These measurements were then used for estimating the laser energy output per pulse exiting the ends of tips, by knowing the energy values coupled into the blunt end of fiber tip. Introduction of the ablated materials into the mass spectrometer was performed using a sampling capillary. The relative positioning of this sampling capillary with respect to the SNOM tip and the sample surface was done using a micromanipulator (Nikon Narishige MO-338, Tokyo, Japan), and is crucial for the analyte detection, as described elsewhere [26, 27].

Unless otherwise noted, all chemicals and materials were purchased at the highest available quality from Fluka (Buchs, Switzerland) and used without any further purification. Tris(8-hydroxyquinolinato)aluminum (Alq_3) and anthracene pellets were pressed from fine powders using a hydraulic press. The powders were pressed by applying a force of about 1×10^5 N for 20 min.

As mentioned above, SNOM tips with wide cone angles were produced by raising the temperature of the etching solvent. It is found that there is a nearly linear relationship between the tip cone angle and the temperature in the range from 20 to 45 °C, as shown in Fig. 1b. As proposed in the convection mechanism of tubing etching, the higher diffusion rate of products and reactants at higher temperature should lead to a more isotropic etching profile, thus a wider tip cone angle [47]. On the other hand, a higher fiber etch rate, caused also by the temperature rise, should generate sharper tips [47]. The increase of diffusion rate apparently dominates, resulting in increased cone angles with higher etching temperature [47]. The surface of tips etched at 60 °C became very rough; thus, etching at higher temperatures was not performed. In terms of laser throughput, mechanical stability, and smoothness of the tip surface, the tips etched at 45 °C represented the best compromise (average cone angle around 40°) and were chosen for this study. An SEM image of a representative tip etched at 45 °C is presented in Fig. 1c. It shows a clean and smooth surface, except for a few particles left. Instead of metal-coated tips which were used in our previous publications [27], uncoated tips were used for this study because their clean and smooth surfaces are ideal for the observation of material redeposition from laser ablation events, while the surface of coated tips would be more problematic for distinguishing redeposited material. It is known that light leakage out of uncoated tip cones is much larger and that tip damage occurs more easily [49]. However, the relatively low laser energies we used and the fact that submicrometer craters can be routinely produced rendered uncoated tips the choice for our study. We are aware of the fact that for generating even smaller craters several tens of nanometers in diameter coated tips would be necessary.

Results and discussions

Tips produced using the "tube etching" method are known for routinely possessing quite smooth surfaces [47]. SEM images of the tips were always obtained before and after the laser ablation experiments for the purpose of comparison. Some control experiments were performed to rule out possible false positives. For example, SEM images of the

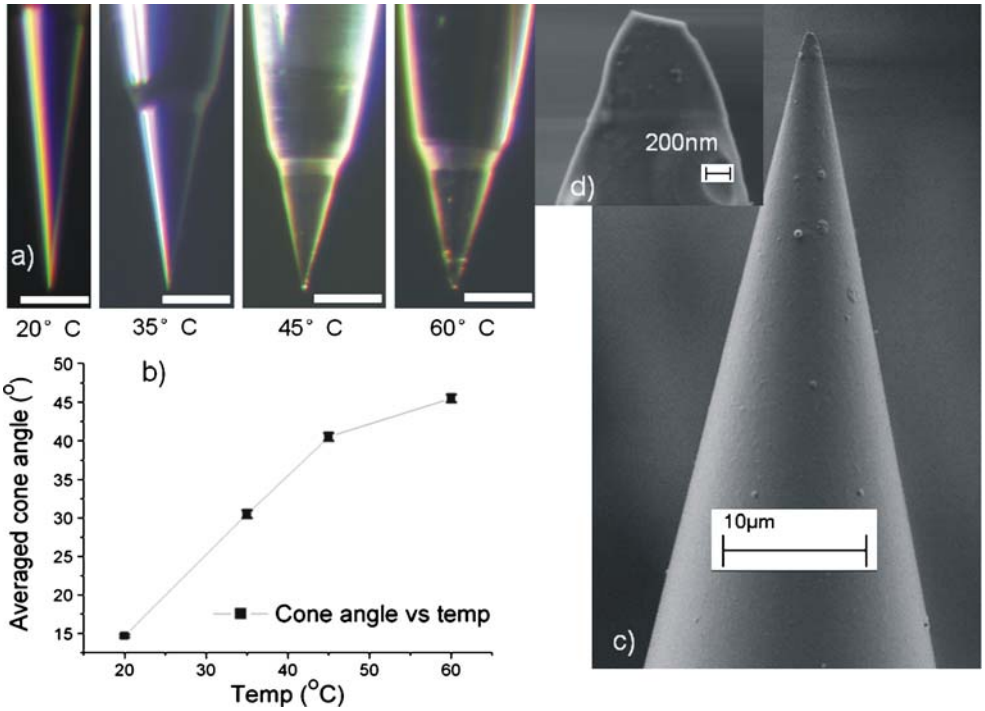

Fig. 1 **a** Optical microscopy images (magnification ×63, *scale bar*=50 μm) of four SNOM tips etched at different temperatures. **b** Relationship between the tip cone angle and the etching temperature in the range from 20 to 60 °C, determined from three tips etched at each temperature. **c** SEM image of one tip etched at 45 °C, showing a rather smooth surface except for a few particles. **d** Zoomed-in view of the tip end, showing an apex diameter around 300 nm

tips after topographic scanning of the surface only (without laser ablation) were taken, and it was observed that the surface of these tips was the same as before scanning, with the exception of the very end of the tip, which sometimes was contaminated by material collected from the sample surface during scanning. The material collected purely by scanning was located within ~1–4 μm from the tip apex and the shape of the collected material was distinctly different from redeposited matter generated by laser ablation events.

Laser ablation on anthracene sample surfaces

First, the optimum laser energy to give appropriate crater size was determined for individual uncoated SNOM tips on each substrate. For this purpose, a 10×10 μm^2 area was scanned before and after individual laser ablation events with defined laser energies to measure the crater profiles. Based on these results, laser energies around ~10–15 nJ per pulse (corresponding to ~$0.8–1.2\times10^5$ W/cm^2, estimated for a laser pulse width with 10 ns and an illuminated area with 1 μm diameter) were found to be suitable for generating craters with single shot, as shown in Fig. 2b. The laser energy is of the same order as the estimated energy needed for material desorption: using a conical crater (r=~0.5 μm and depth=~0.5 μm) and a sublimation energy for anthracene of 52.5 kJ/mol, we calculated that ~5 nJ would be needed to desorb all the material from the crater. Generally, somewhat larger craters with diameters around 1 μm were produced, in order to accumulate more material on the tip surface for a clearer visualization. An improvement of the spatial resolution from 5 to 1 μm (assuming the same crater depth) requires about 25 times more sensitivity for detection by MS. Therefore, for our instrument, measuring mass spectra from ~1 μm crater is logically the first step towards measurement below diffraction limit. After the optimum laser energy had been determined, 400 laser ablations were performed on the surface of an anthracene pellet, by laser ablation at 2 Hz during tip scanning (scan rate 10 μm/s, 100×100 pixels). SEM characterization of the tip surfaces clearly showed redeposited material, confined to an area no more than ~20–30 μm from the tip end, as shown in Fig. 2e, g. The large irregular particles ~3–4 μm from the tip apex could be dust collected from the sample surface during scanning. To rule out the possibility that the wide angle tip body prevented the propagation of ablation plume, sharp tips with cone angle less than 10° were also used. Theoretical models propose that the spreading angle of conventional far-field laser ablation plumes is around 10° [45] or even larger [32, 42, 50]. It was observed that the material redepositions on the surface of sharp tips were also confined to ~25 μm from the tip end (data not shown). Thus, it can be concluded the major part of the NF-LA plume propagates a distance of only ~30 μm from the surface, much smaller than in the case of far-field laser ablation [30, 42]. Taking a closer look at the redeposited material on the surface of wide-angle tips for the case of the anthracene pellet, a smooth thin film of redeposited material, embedded in which were many long "islands," can be observed (Fig. 2f). The shape of the islands seems

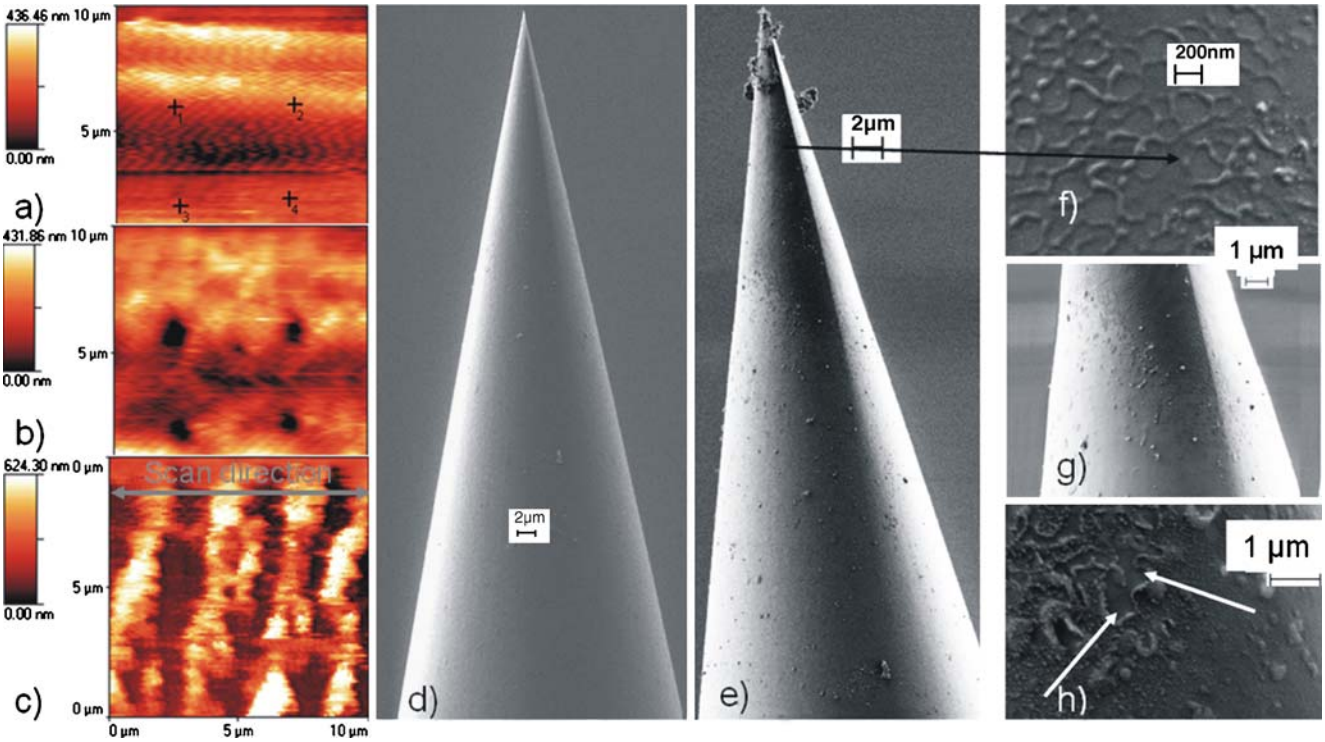

Fig. 2 **a** A 10×10 µm^2 area of an anthracene pellet surface scanned before laser ablation. The four *plus* symbols represent the positions where four single shot laser ablations were performed. **b** The same area scanned after four near-field tip ablation events with ~10 nJ per pulse laser energy, exhibiting craters with a size around 1 µm. **c** Surface topography after scanning while performing laser ablations at 2 Hz with ~10 nJ per pulse laser energy during tip scanning. **d** SEM image of one tip before ablation and scanning. **e** SEM image of the same SNOM tip after 400 laser shots with a laser energy of ~10 nJ per pulse on an anthracene pellet surface. **f**, **g** Zoomed-in view of the tip near its apex, showing a thin film embedded with long islands. **h** Zoomed-in view of another tip after 400 laser shots with a laser energy of ~53 nJ per pulse, showing peeling off of the redeposited thin film near the tip apex. The *white arrows* point to the clean tip surface after the rupture and the peeling off of redeposited thin film

regular and smooth, which may indicate that they originated from condensation of ablated molecules/tiny clusters (aggregates of molecules) instead of ejected particles (with diameter >10 nm). One could also speculate that particles/large clusters were ejected from the molten substrate following laser irradiation and splashed onto the tip surface to generate such structures. However, in this case, the islands should be distinct and separated from each other rather than showing the network structure. The observed network structure is more compatible with "islands" formed gradually by condensation of ablated molecules/tiny clusters (Fig. 2f). Indeed, larger clusters or particles ejected in the molten state from a metallic sample surface, as shown in [35] and [51], should look like regular spherical particles with diameter bigger than several tens of nanometers attached to the sample surface. To further confirm that the smooth thin film originated from ablated molecules/tiny clusters, a higher laser energy (~53 nJ per pulse) was used. Consequently, larger craters were generated and more material was deposited onto the tip surfaces. More importantly, the heating effect around the tip end induced by the cutoff of light propagation [52] caused peeling off of the redeposited thin film near the tip apex, as shown in Fig. 2h. Another observation is that, for this high laser energy ablation, there were not many particles larger than 50 nm. All these observations support the idea that most of the ablated material from submicrometer craters on an anthracene pellet surface is in the forms molecules/tiny clusters (aggregates of molecules), as opposed to giant clusters and particles (referred to size more than 50 nm), and that the near-field ablation plume propagates no more than 30 µm from the sample surface. The above conclusions are also true for the case when bursts of 20 shots with less laser energy (~3–6 nJ output) were used to generate craters of similar size on the anthracene pellet surface, instead of single shot. Furthermore, taking a single crystal of anthracene as the substrate and then following the above-mentioned procedures, the redeposited anthracene on tip surfaces appears similar, suggesting the absence of a possible influence from the sample morphology (data not shown).

An important question concerns the ratio of redeposited to ablated material. This can be roughly estimated. A smooth anthracene surface area of 10×10 µm was scanned before and after 400 single laser shots delivered at 2 Hz

during the scanning of the tip. The scan rate was 10 μm/s and the number of pixels per line was 100. The laser energy coupled into the fiber tip was high enough to generate craters of ≤1 μm diameter with a single shot. As shown in Fig. 2c, there were four trenches formed after the tip scanning process, two during forward scans, and the other two during the reverse scans. The firing of the laser events in the experiments was synchronized to the tip scan. Taking the average depth of these trenches as ~0.6 μm, the average width as ~0.86 μm, and their length as 10 μm, the total ablated volume is calculated to be 20.64 μm^3. For the material redeposition on the tip surface, the thickness of the thin film varies with position. To define low/high estimates, both the thickness of the thinnest part (~10 nm, estimated thickness of thinnest film from the edge of the redeposited film where the film ends) and the thickest part (~50 nm, estimated thickness of thickest film from an area where the redeposited film was ruptured) were taken to calculate the volume the redeposited material on the tip surface. The end of the tip was regarded as a regular circular cone with a base radius of ~4 μm and slant height of ~22.4 μm. We could derive that roughly 13% (from the thinnest part of the film) to 70% (from the thickest part of the film) of the ablated material is redeposited on the tip surface. In other words, material redeposited on the tip represents a substantial amount, which needs to be taken into account when calculating the detection efficiency in near-field laser ablation mass spectrometry coupled with SPM-based (either aperture or apertureless) techniques. Material redeposition on the sample surface was not taken into account because its extent is difficult to be estimated but will only represent further losses in sample transport. To simplify matters, we calculated the volume instead of the mass here, in order to avoid difficulties in estimating the density difference between the ablated and redeposited material.

The short height of the near-field ablation plume (about ~20–30 μm) emphasizes the importance of the positioning of the MS sampling capillary whose active suction range is estimated to roughly equal to be its internal diameter (~250 μm) close to the ablation site and the end of the SNOM tip. Also, MS signals could be generated from desorption of redeposited material on the tip surface instead of material ablated directly from the sample surface, especially when using a higher laser energy intended to ablate more material from the sample. After using some tips for ablation several tens of times, the accumulated material on the tip surface and the short distance between the tip itself and the orifice of the sampling capillary could amplify this effect. When such a tip is used to ablate different materials, contamination caused by redeposition on the tip surface also needs to be taken care of, especially if quantitative analysis is required.

Laser ablation on Alq_3 sample surfaces

Alq_3 is a common component of organic light-emitting diodes (OLED) with the formula $Al(C_9H_6NO)_3$. The investigation of its behavior in laser ablation is not only important for characterizing laser ablation mass spectrometric methods and for the further analysis of OLED microstructures and nanostructures but also interesting for the deposition of Alq_3 using pulsed laser deposition (PLD) or pulsed laser evaporation techniques [53, 54].

In this study, an Alq_3 pellet pressed from fine powder was taken as the substrate and the wide-angle tips (~40°) shown above were utilized. Following the protocol introduced before, the optimum laser energy to produce one crater with ~1 μm diameter was first determined. As shown in Fig. 3b, single-shot laser ablation using an SNOM tip with ~15 nJ per pulse laser energy generates craters with ≤1 μm diameter in a point-to-point mode. Afterwards, by scanning a $10 \times 10\ \mu m^2$ surface with scan rate of 10 μm/s and pixel size of 0.1 μm, a total of 400 shots were delivered during the whole scan, while the laser repetition rate was set to 2 Hz. After these 400 shots, the tip was characterized with SEM, as shown in Fig. 3d (overview). The comparison with the SEM image of the same tip before any laser ablation shows clearly that there was material redeposited in various forms up to a height of ~50 μm. The redeposited material could be identified as Alq_3 by analyzing the elemental composition with energy-dispersive X-ray emission coupled to the SEM (data not shown). As opposed to the simple form of redeposited anthracene, the shape of redeposited Alq_3 varies from region to region. The area in Fig. 3e is the one closest to the tip apex. In that region, the coverage on the tip surface is interpreted as a molten rough film with holes, which is a clear indication of a tip heating effect induced by the laser. More interestingly, the region of this rough film ends around 10 μm from the end of the tip, which is consistent with the distance at which failure of etched SNOM tips by laser-induced melting has been reported [55]. This is corroborating experimental evidence to show how much heating the apex area of the SNOM probe actually experiences and could also be used for indirect estimation of heating effects on the sample surface, which is only 10 nm away from the tip apex. Further up from the rough area (between 10 and 30 μm from the tip apex), the tip surface was covered with a thin film probably condensed from ablated molecules/tiny clusters, on top of which there were particles and even agglomerated particles with a size from ~50 to 100 nm attached. The particles seen in Fig. 3f are most likely from ejection of material in the molten state from the sample surface since their shapes are regular and spherical, similar to the discussions in [35] and [51]. These ejected molten particles were not seen on the tip surface further up,

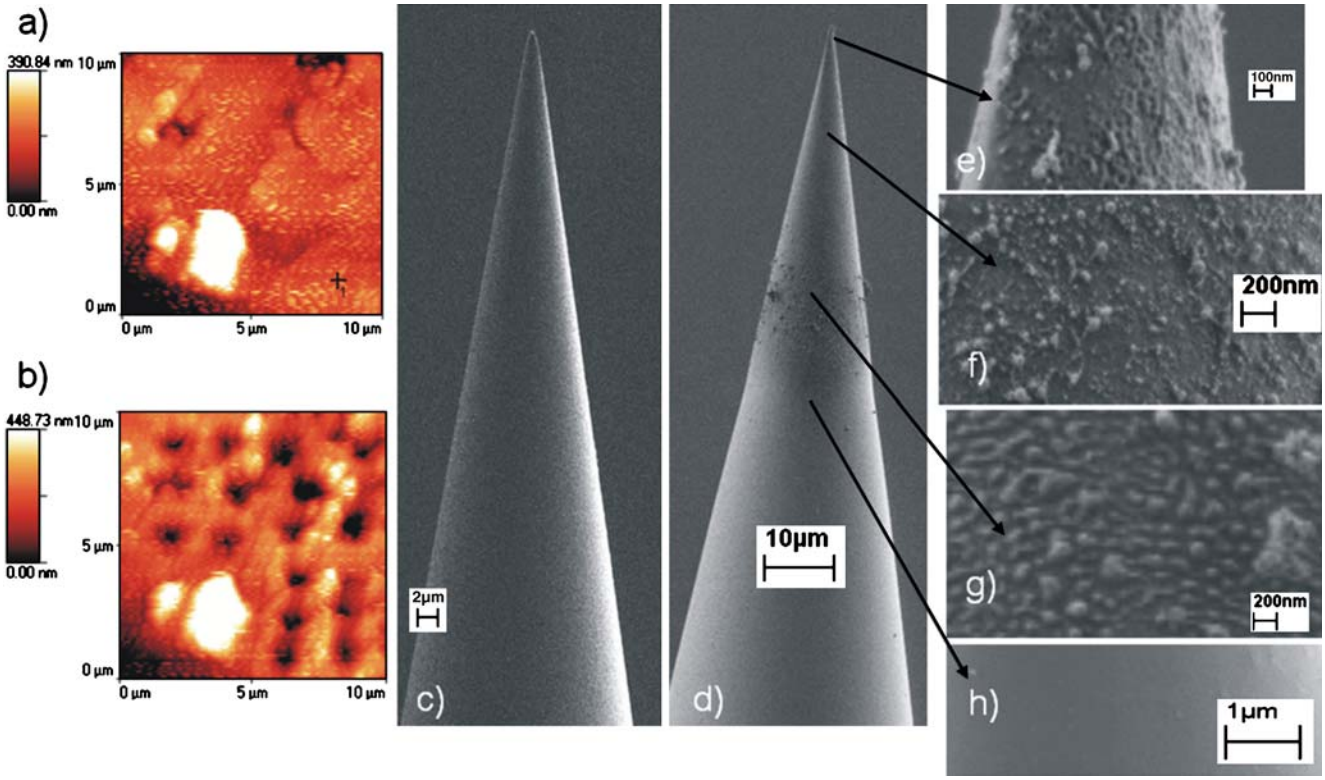

Fig. 3 **a** A 10×10-µm^2 area of an Alq_3 pellet surface scanned before laser ablation. **b** The same area scanned after 16 ablation events with ~15 nJ per pulse laser energy, exhibiting craters with a size around 1 µm. **c** SEM image of one tip before ablation and scanning. **d** SEM image of the same SNOM tip after 400 laser shots of ~15 nJ per pulse laser energy delivered onto an Alq_3 pellet surface. **e**–**g** Zoomed-in views of the tip surface at different distances from the end of the tip, showing redeposited Alq3 in various forms. **h** Zoomed-in view of the tip surface 50 µm from the end of the tip, showing no material redeposition

~40 µm away from the tip apex, shown in Fig. 3g. Instead, there were almost only structures reminiscent of condensed molecules/tiny clusters. Furthermore, some irregular particles were also found at a distance far from the tip apex (>40 µm). These particles could have been ejected directly from the surface. The observation of various forms of redeposited material at different locations could be linked to the two phase laser ablation theory which proposes the presence of two laser plume components [42]. According to this theory, a fast component composed mainly of gaseous neutrals and tiny clusters is generated several tens of nanoseconds after the laser pulse [42]. The ejected molten particles with a much slower expansion velocity are the major part of the second plume component, which remains closer to the sample surface even after tens of microseconds [42, 45, 46]. It seems that this structure of the laser ablation plume was kept in the near-field case but in a much smaller dimension. That could be the reason why the ejected molten particles can only be observed until a height of ~25 µm while the thin film condensed out of ablated molecules/tiny clusters was found higher above the sample surface. Of course, one difference, given by the special geometry used here, is the area near the tip apex, where the redeposited material could be heated or even again "cleaned off" by laser coupled in. The differences in timescale need to be further pursued using real-time imaging techniques.

In the future, the structures of Alq_3 redeposited in different tip areas could be analyzed in more detail by studying the corresponding photoluminescence spectra. This could be done by coupling a well-focused light beam into the SEM.

Plume propagation on tilted sample surfaces

In PLD applications, the target is normally parallel to the collection substrate but tilted with respect to the laser beam. Theoretical predictions suggest that ablation plumes in PLD applications propagate normal to the target surface [56]. Although it has been found experimentally that the plume propagation is tilted towards the axis of incident laser beam [57–59], this deflection depends on two essential requirements: a rough morphology of the target film and a large number of shots (e.g., hundreds of pulses [56]) at the same location. Thus, plume deflection should not be observed in our case since we always employ single shots or a maximum of five shots at each spot. In our recent NF-LA MS experiments[27], the sample was fixed onto a glass

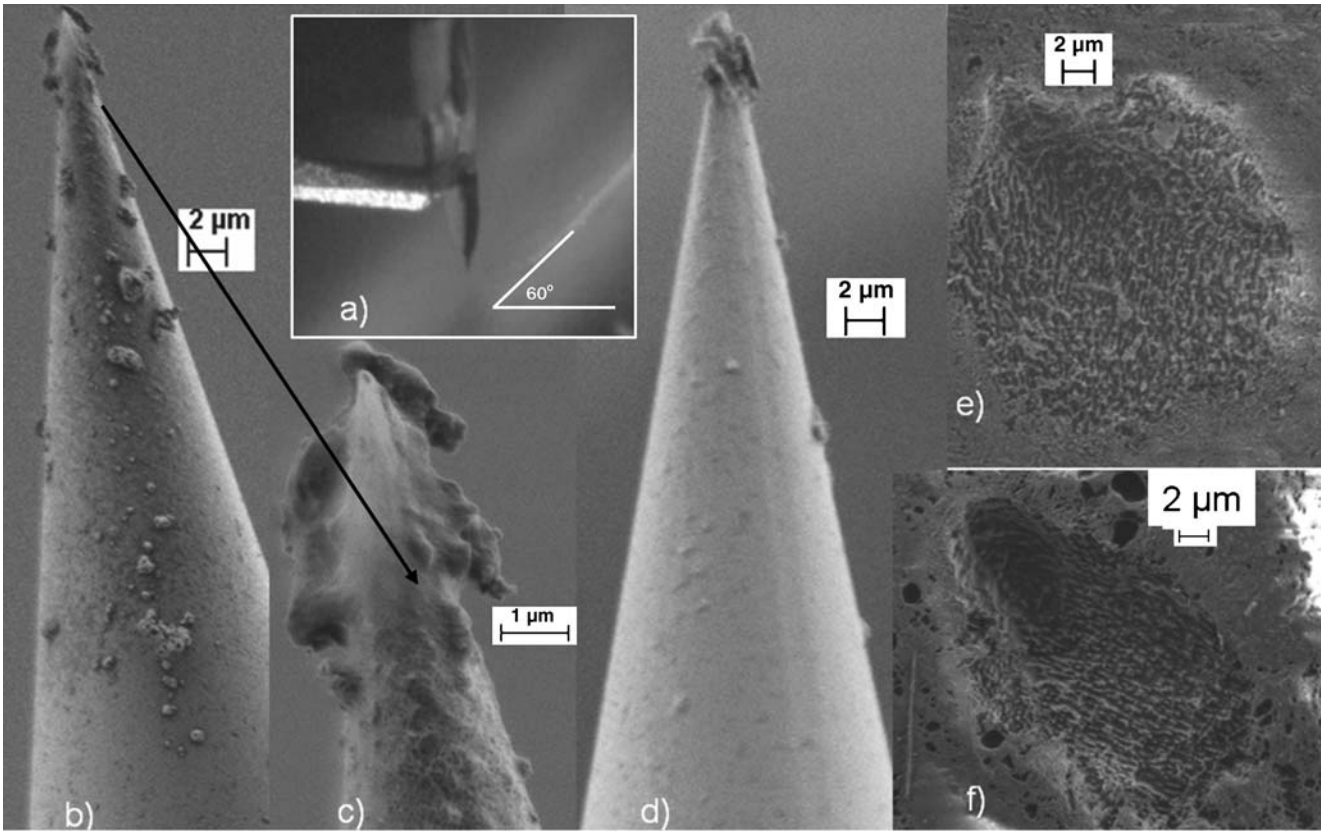

Fig. 4 **a** Side view of a SNOM tip vertically approached on a tilted sample surface by 60° from the horizontal surface, the symbol of 60° shown to guide the eyes. **b** SEM images of a SNOM tip after 300 laser shots with 10-nJ laser energy delivered onto an anthracene pellet surface. The surface shown here is the one facing the substrate surface during laser ablation. **c** Zoomed-in view of the tip apex. **d**. SEM image of the back side of the same tip. **e**, **f** SEM images of craters ablated at the nontilted surface and tilted surface, respectively

slide on a simple solid sample holder that is tilted by 15° for better sampling efficiency: a tilted surface not only allows positioning the sampling capillary closer to the SNOM tip but is also expected to direct the laser ablation plume into the direction where the sampling capillary is located [27]. However, does the plume still propagate normal to the surface in near-field events? In the present study, an anthracene pellet was mounted on the sample holder which was tilted by 60° from the horizontal. The SNOM tip was then vertically approached to the sample surface, as shown in Fig. 4a. Since scanning cannot be performed on such a steep surface, about 300 laser ablations were done in point-to-point mode. Based on previous measurements, ~10 nJ per pulse was used for these 300 laser shots. Afterwards, the tips were checked using SEM, and one of them is shown in Fig. 4b, c. The surface of the tip seen in these two images is the one facing the anthracene pellet surface during laser ablation. Compared to the SEM picture of the back surface (Fig. 4d), the difference in the amount and distribution of redeposited material is clear. Indeed, there is almost no material collected at the back side of the tip. The distinct inhomogeneity of material redeposition clearly demonstrates that the laser plume does not follow the incident laser direction, consistent with previous discussions. Some more evidence can be found in Fig. 4e, f which is SEM images of craters ablated at nontilted vs tilted surface with higher laser energies, respectively. As can be seen from Fig. 4e, the crater on the nontilted substrate is fairly circular and regular, while the crater generated on the tilted surface is more inhomogeneous. The deepest part of the crater in Fig. 2f is probably the position where the SNOM tip was approached. The fan-shaped area suggests that the plume was not normal to the surface but deflected away from the surface normal, opposite to the direction of the incoming laser direction. This behavior of plume propagation supports the assumption in our previous publication [27] and can be exploited to direct ablated material, thus facilitating more efficient sampling of ablated products for mass spectrometric analysis.

Conclusions and outlook

Although the complicated chemical and physical processes underlying near-field laser ablation on molecular solids at

atmospheric pressure prevent a detailed understanding of the nature of the event, the characterization of the SNOM tips after laser ablations with different laser conditions on the surface of both anthracene and Alq_3 pellets using SEM allows some fundamental insight into near-field laser ablation events. This knowledge is not only useful for optimizing near-field laser ablation mass spectrometric methods but also of general interests for applications such as PLD at smaller dimension. In the next step, we propose to study the effect of laser pulse width (for e.g., nanosecond laser vs femtosecond laser) due to the advantage of less material damage by ultrashort pulses.

Characterization of the SNOM tip surface using SEM has proven to be an efficient method to gain some fundamental insight during near-field laser ablation events on various molecular solid surfaces under different laser conditions. Near-field ablation with aperture-based SNOM tips yielding craters of ≤1 μm diameter has clearly demonstrated that (1) there is a considerable amount of ablated material redeposited on the SNOM tip. The ratio of the redeposited material to the amount of ablated material could be as high as 70%. Most of the materials ablated from anthracene surfaces were in the form of molecules/tiny clusters (aggregates of molecules), while, for the case of Alq_3, particulates with a size from tens to hundreds of nanometers were also generated. (2) The propagation of most material in the near-field ablation plume stops at a height around ~50 μm from both the anthracene and Alq_3 surface, which emphasizes the importance of the relative positioning between the sampling capillary, the SNOM tip, and the sample surface in NF-LA MS. (3) Observations of tips after ablation of an anthracene surface angled at 60° with respect to the horizontal direction support the hypothesis that the near-field ablation plume is neither in the direction of the surface normal nor towards the axis of incident laser beam but deviates further away from surface normal, opposite to the direction of the incoming laser direction. If the MS sampling geometry is adapted based on the above findings, improvements in sensitivity are to be expected.

Acknowledgement SEM was carried out at EMEZ (electron microscopy ETH Zurich).

References

1. Bailo E, Deckert V (2008) Chem Soc Rev 37:921–930
2. Yeo BS, Madler S, Schmid T, Zhang WH, Zenobi R (2008) J Phys Chem C 112:4867–4873
3. Zhang WH, Yeo BS, Schmid T, Zenobi R (2007) J Phys Chem C 111:1733–1738
4. Betzig E, Trautman JK, Harris TD, Weiner JS, Kostelak RL (1991) Science 251:1468–1470
5. Klar TA, Jakobs S, Dyba M, Egner A, Hell SW (2000) Proc Natl Acad Sci U S A 97:8206–8210
6. Dunn RC (1999) Chem Rev 99:2891–2992
7. McDonnell LA, Heeren RMA (2007) Mass Spectrom Rev 26:606–643
8. Laiko VV, Baldwin MA, Burlingame AL (2000) Anal Chem 72:652–657
9. Laiko VV, Taranenko NI, Berkout VD, Yakshin MA, Prasad CR, Lee HS, Doroshenko VM (2002) J Am Soc Mass Spectrom 13:354–361
10. Jurchen JC, Rubakhin SS, Sweedler JV (2005) J Am Soc Mass Spectrom 16:1654–1659
11. Koestler M, Kirsch D, Hester A, Leisner A, Guenther S, Spengler B (2008) Rapid Commun Mass Spectrom 22:3275–3285
12. Chaurand P, Schriver KE, Caprioli RM (2007) J Mass Spectrom 42:476–489
13. Luxembourg SL, Mize TH, McDonnell LA, Heeren RMA (2004) Anal Chem 76:5339–5344
14. Spengler B, Hubert M (2002) J Am Soc Mass Spectrom 13:735–748
15. Altelaar AFM, Taban IM, McDonnell LA, Verhaert P, de Lange RPJ, Adan RAH, Mooi WJ, Heeren RMA, Piersma SR (2007) Int J Mass Spectrom 260:203–211
16. Heeren RMA, Altelaar AFM, Taban IM, McDonnell LA, Verhaert PDEM, de Lange RPJ, Adan RAH, Mooi WJ, Piersma SR (2007) Int J Mass Spectrom 260:203–211
17. Sherrod SD, Castellana ET, McLean JA, Russell DH (2007) Int J Mass Spectrom 262:256–262
18. Touboul D, Halgand F, Brunelle A, Kersting R, Tallarek E, Hagenhoff B, Laprevote O (2004) Anal Chem 76:1550–1559
19. Dutoit B, Zeisel D, Deckert V, Zenobi R (1997) J Phys Chem B 101:6955–6959
20. Zeisel D, Nettesheim S, Dutoit B, Zenobi R (1996) Appl Phys Lett 68:2491–2492
21. Meyer KA, Ovchinnikova O, Ng K, Goeringer DE (2008) Rev Sci Instrum 79:123710
22. Chimmalgi A, Choi TY, Grigoropoulos CP, Komvopoulos K (2003) Appl Phys Lett 82:1146–1148
23. Zoriy MV, Becker JS (2009) Rapid Commun Mass Spectrom 23:23–30
24. Zoriy MV, Kayser M, Becker JS (2008) Int J Mass Spectrom 273:151–155
25. Stöckle R, Setz P, Deckert V, Lippert T, Wokaun A, Zenobi R (2001) Anal Chem 73:1399–1402
26. Setz PD, Schmitz TA, Zenobi R (2006) Rev Sci Instrum 77:9
27. Schmitz TA, Gamez G, Setz PD, Zhu L, Zenobi R (2008) Anal Chem 80:6537–6544
28. Georgiou S, Koubenakis A (2003) Chem Rev 103:349–393
29. Handschuh M, Nettesheim S, Zenobi R (1999) Appl Surf Sci 137:125–135
30. Perez D, Lewis LJ, Lorazo P, Meunier M (2006) Appl Phys Lett 89:141907
31. Jackson SN, Kim JK, Laboy JL, Murray KK (2006) Rapid Commun Mass Spectrom 20:1299–1304
32. Apitz I, Vogel A (2005) Appl Phys A Mater Sci Process 81:329–338
33. Samek O, Kurowski A, Kittel S, Kukhlevsky S, Hergenroder R (2005) Spectrochim Acta B At Spectrosc 60:1225–1229
34. Garcia CC, Lindner H, Niemax K (2009) J Anal At Spectrom 24:14–26
35. Hergenröder, R (2006) Spectrochim Acta B At Spectrosc 61:284–300
36. Hergenröder R (2006) J Anal At Spectrom 21:1016–1026
37. Koch J, Schlamp S, Rosgen T, Fliegel D, Gunther D (2007) Spectrochim Acta B At Spectrosc 62:20–29
38. Koch J, Walle M, Schlamp S, Rosgen T, Gunther D (2008) Spectrochim Acta B At Spectrosc 63:37–41

39. Koch J, We M, Dietiker R, Gunther D (2008) Anal Chem 80:915–921
40. Pisonero J, Gunther D (2008) Mass Spectrom Rev 27:609–623
41. Fernandez B, Claverie F, Pecheyran C, Donard OFX (2007) Trends Anal Chem 26:951–966
42. Itina TE, Povarnitsyn ME, Gouriet K, Noel S, Hermann J (2007) Photon Processing in Microelectronics and Photonics VI 6458:U4581
43. Zhigilei LV, Leveugle E, Garrison BJ, Yingling YG, Zeifman MI (2003) Chem Rev 103:321–347
44. Chen ZY, Vertes A (2008) Phys Rev E 77:036316
45. Hirata T, Miyazaki Z (2007) Anal Chem 79:147–152
46. Hopp B, Kresz N, Vass C, Toth Z, Smausz T, Ignacz F (2001) Appl Surf Sci 186:298–302
47. Stöckle R, Fokas C, Deckert V, Zenobi R, Sick B, Hecht B, Wild UP (1999) Appl Phys Lett 75:160–162
48. Arslanov NM (2006) J Opt A Pure Appl Opt 8:338–344
49. Thiery L, Marini N (2003) Ultramicroscopy 94:49
50. Conde JC, Lusquinos F, Gonzalez P, Serra J, Leon B, Cultrera L, Guido D, Perrone A (2004) Appl Phys A Mater Sci Process 79:1105–1110
51. Gonzalez JJ, Liu CY, Wen SB, Mao XL, Russo RE (2007) Talanta 73:567–576
52. Larosa AH, Yakobson BI, Hallen HD (1995) Appl Phys Lett 67:2597–2599
53. Pique A, Wu P, Ringeisen BR, Bubb DM, Melinger JS, McGill RA, Chrisey DB (2002) Appl Surf Sci 186:408–415
54. Yang XJ, Tang YX, Yu M, Qin QZ (2000) Thin Solid Films 358:187–190
55. Dickenson NE, Erickson ES, Mooren OL, Dunn RC (2007) Rev Sci Instrum 78:053712
56. Cultrera L, Zeifman MI, Perrone A (2007) Appl Surf Sci 253:6322–6325
57. Aksouh F, Chaurand P, Deprun C, Dellanegra S, Hoyes J, Lebeyec Y, Pinho RR (1995) Rapid Commun Mass Spectrom 9:515–518
58. Anisimov SI, Bäuerle D, Lukyanchuk BS (1993) Phys Rev B 48:12076–12081
59. Ayala E, Vera CC, Hakansson P (1999) Rapid Commun Mass Spectrom 13:792–797